

# The influence of the segregation of Cu-rich phase on the microstructural and impedance characteristics of $\text{CaCu}_3\text{Ti}_4\text{O}_{12}$ ceramics

B. Shri Prakash · K. B. R. Varma

Received: 29 June 2006 / Accepted: 10 November 2006 / Published online: 18 May 2007  
© Springer Science+Business Media, LLC 2007

**Abstract** The influence of sintering conditions on the microstructural features and impedance characteristics of the giant dielectric constant material  $\text{CaCu}_3\text{Ti}_4\text{O}_{12}$  (CCTO) was investigated. The microstructure and impedance characteristics were found to be strongly dependent on the sintering conditions. Sintering of the CCTO ceramics at elevated temperatures ( $>1100^\circ\text{C}$ ) for prolonged durations resulted in the segregation of Cu-rich phase, mostly confined to the surface, which was in concomitance with the appearance of the additional semicircle at the low frequency end in Impedance ( $Z^*$ ) plots. The absence of this additional semicircle in the Cu-deficient CCTO ceramics and the appearance of the same in Cu-rich CCTO ceramics that were deliberately fabricated corroborated the above observations. Also,  $\text{La}_{2/3}\text{Cu}_3\text{Ti}_4\text{O}_{12}$  (LCTO), a low dielectric constant member of CCTO family, which consisted of small grains without the segregation of Cu-rich phase at the grain boundary, did not reveal the presence of additional semicircle in the  $Z^*$  plots.

## Introduction

Materials with high relative dielectric constant, low loss, and a low-temperature coefficient of the dielectric constant have been the subject of extensive research as these play an important role in the electronic devices [1–5]. The main focus has been on perovskite based ferroelectric materials,

owing to their high intrinsic dielectric constant originating from the dipolar polarization in addition to the electronic and ionic polarization [6]. However, the dielectric properties of these materials are strongly temperature dependent and undergo a maximum in the vicinity of the ferroelectric to paraelectric transition temperature [6]. These characteristics are undesirable from the viewpoint of electronic device applications. In this context, the discovery of an unusual cubic perovskite material  $\text{CaCu}_3\text{Ti}_4\text{O}_{12}$  (CCTO) has generated immense interest due to its giant dielectric constant ( $>10^4$ ) despite its centrosymmetric space group ( $\text{Im}3$ ) [7–11]. The polycrystalline CCTO was reported to exhibit a remarkably high room temperature dielectric constant of  $>10^4$  at 100 kHz [7–9]. However, the dielectric constant was strongly dependent on the processing conditions [11–13]. Further, the dielectric constant was reported to remain constant in the 100–400 K temperature range. When the temperature was lowered below 100 K, the dielectric constant decreased by three orders of magnitude ( $<100$ ) [7–9]. However, neither a phase transition nor a detectable change in the long-range crystal structure was found by high resolution X-ray and neutron diffraction studies in the 100–600 K temperature range [7, 8]. In the frequency domain, it showed an extremely high value of dielectric constant ( $>10^4$ ) at room temperature in the 100 Hz–1 MHz frequency range and exhibited a dielectric relaxation above this frequency. The value of the dielectric constant above the relaxation frequency was as low as 80 and the frequency of dielectric relaxation was dependent on the measuring temperature [7–11].

Several contradictory models, either based on the intrinsic crystal structure or the extrinsic phenomenon have been proposed to explain the dielectric behavior of CCTO [7–11, 14–18]. However, among these models, at present the internal (grain boundary) barrier layer capacitance

B. Shri Prakash · K. B. R. Varma (✉)  
Materials Research Centre, Indian Institute of Science,  
Bangalore 560012, India  
e-mail: kbrvarma@mrc.iisc.ernet.in

(IBLC) model [10, 11] is widely accepted. This model was based on Impedance Spectroscopy (IS), which revealed CCTO ceramics to be electrically heterogeneous and consisted of semiconducting grains with insulating grain boundaries and attributed the giant dielectric phenomenon to the grain boundary layer capacitance [10, 11]. In these studies, the room temperature impedance plots ( $Z^*$  plots) of CCTO consisted of a Debye-like semicircle with a nonzero intercept on the  $Z'$ -axis at high frequency end. These  $Z^*$  plots were analyzed using a simplified circuit consisting of two parallel RC elements, connected in series, one RC element,  $R_bC_b$ , representing the semiconducting grains and the other,  $R_{gb}C_{gb}$ , representing the insulating grain boundary regions. Based on this equivalent circuit, and in accordance with the brickwork layer model for electroceramics, the large arc observed at low frequency was attributed to the grain boundary response and the nonzero intercept on the  $Z'$  axis at high frequencies was attributed to the bulk resistance,  $R_b$  [10, 11].

Most of the investigations into CCTO, after its dielectric properties were initially reported in the year 2000 [7], have been mainly centered around the low temperature dielectric behavior of the material due to the dielectric anomalies that were exhibited by it in the low temperature region [7–11]. Only a few papers in the recent times have dealt with the high temperature dielectric behavior of CCTO [12, 19, 20]. In one of these studies, an additional dielectric relaxation in the low frequency end at high temperature was observed and was attributed to electrode effects [19]. The work that was published later on the high temperature behavior of CCTO refuted the role of electrode effects on this additional relaxation as no change in the dielectric relaxation strength was observed on using different electrodes [20]. Though there are a few research articles on the high temperature electrical behavior of the title compound, to the best of the knowledge of the present authors, no comprehensive study with regard to the microstructural evolution and the consequent impedance characteristics has been reported in the literature. It is with this background that we have performed a systematic IS study on the samples with varied microstructures. This has led us to establish a direct correlation between the microstructure, composition and the impedance response. In order to obtain ceramics of CCTO with different microstructures, the samples were subjected to various sintering conditions.

## Experimental

Polycrystalline ceramic powder of CCTO was prepared via the conventional solid-state reaction route using stoichiometric amounts of  $\text{CaCO}_3$ ,  $\text{CuO}$ , and  $\text{TiO}_2$ . These were thoroughly mixed in an acetone medium using a ball mill.

This was followed by the calcination of the powder in an Alumina crucible at 1000 °C/10 h with intermittent grinding. The formation of the monophasic compound was confirmed by X-ray powder diffraction (XRD) using  $\text{Cu K}_\alpha$  radiation. The polycrystalline powder was then cold pressed into pellets of 10 mm in diameter and 2 mm in thickness at the pressure of 300 kg/cm<sup>2</sup> using PVA as binder. The pressed pellets were initially heated slowly to 600 °C to get rid of the binder. The first set of pellets were separately sintered in air at 1025, 1050, 1075, 1100 and 1120 °C for 10 h followed by the second set of pellets at 1100 °C for 2.5, 5, 7.5, 10, 15 and 20 h, respectively. Along with these samples, Cu-rich and Cu-deficient samples were also prepared according to the chemical formula  $\text{CaCu}_{3.2}\text{Ti}_4\text{O}_{12}$  and  $\text{CaCu}_{2.8}\text{Ti}_4\text{O}_{12}$ . These pellets were sintered at 1100 °C for 10 h. In addition, a pellet of  $\text{La}_{2/3}\text{Cu}_3\text{Ti}_4\text{O}_{12}$  (LCTO) was prepared using  $\text{La}_2\text{O}_3$ ,  $\text{CuO}$  and  $\text{TiO}_2$  and was sintered at 1100 °C/40 h. XRD studies were carried out on the sintered pellets also to confirm the retention of the monophasic nature of the pellets after sintering.

Microstructure and the grain size distribution in different samples were studied using Scanning electron microscopy (SEM). Elemental analysis was carried out using the Energy dispersive X-ray analysis (EDX) associated with the SEM. The SEM pictures were taken both in the secondary electron and back scattered modes to identify the compositional inhomogeneity. Elemental mapping was performed on selected areas of sintered samples to know the distribution of individual cations on the surface. The SEM, EDX analyses and elemental mapping were carried out on the fractured surfaces to visualize the morphology and also to probe the composition into the bulk of the sample as well.

To make electrical measurements, gold electrodes were sputtered on to the pellet surfaces and copper wires were glued on to the gold-coated surfaces using silver paste. Capacitance measurements were carried out on the ceramic samples as a function of frequency (100 Hz–1 MHz) in the 30–250 °C temperature range using the impedance gain phase analyzer (HP4194A) at signal strength of 0.5  $V_{\text{rms}}$ .

## Results and discussion

The XRD powder patterns obtained for CCTO ceramic powder and for the CCTO pellets that were sintered at different temperatures are shown in Fig. 1a–d. The diffraction pattern obtained for the ceramic powder could be indexed to a body-centered cubic perovskite related structure of space group  $\text{Im}\bar{3}$ . The XRD powder patterns obtained for 1000 °C/10 h calcined CCTO (Fig. 1a) and for the pellets sintered at 1050 °C/10 h (Fig. 1b) are similar

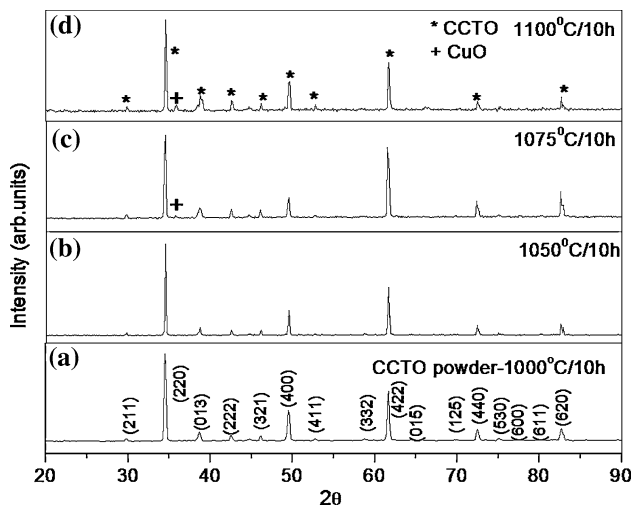


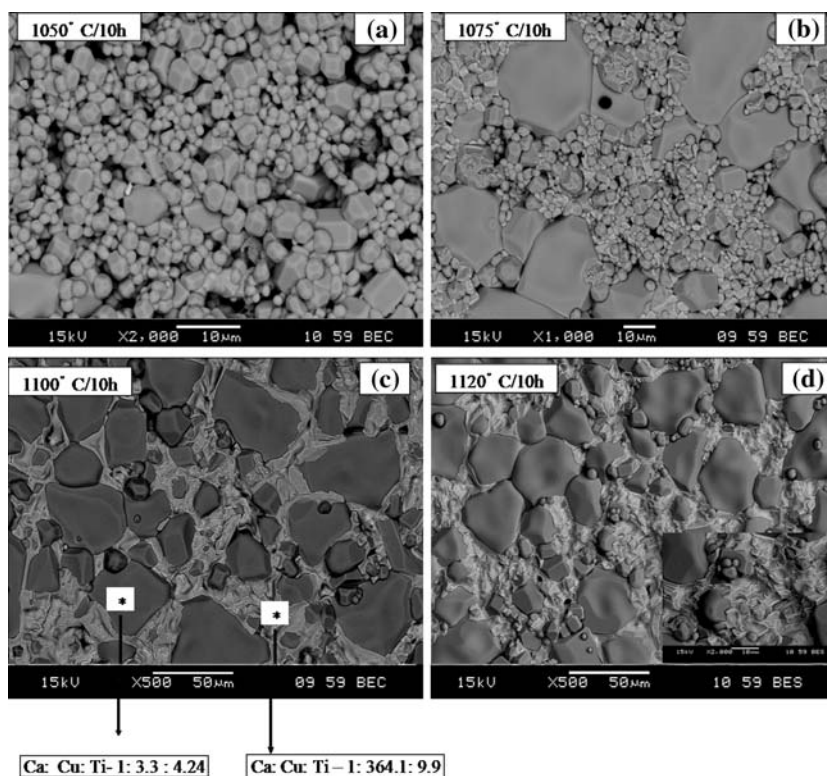
**Fig. 1** XRD powder patterns for (a) CCTO powder calcined at 1000 °C/10 h and for the specimens sintered at different temperatures (b) 1050 °C/10 h (c) 1075 °C/10 h (d) 1100 °C/10 h

wherein there is no detectable secondary phase. However, on increasing the sintering temperature to 1075 °C and above, a secondary peak corresponding to CuO (indicated by +) appears, and its intensity increases with increase in the sintering temperature (Fig. 1c, d). A similar trend is observed even for the second set of pellets sintered at 1100 °C for different durations. The XRD pattern (Not shown in the figure) obtained for the pellet sintered at

1100 °C for 2.5 h and 5 h are similar with no noticeable CuO phase present. The additional peak corresponding to CuO appears on increasing the sintering duration further.

The Scanning electron micrographs of the CCTO pellets revealing the microstructural evolution on increasing the sintering temperature are depicted in Fig. 2a–d. The micrograph of the pellet sintered at 1050 °C/10 h shows the initiation of the discontinuous grain growth with an average grain size of 3–5 μm (Fig. 2a). The back-scattered image of the pellet reveals that the composition is nearly uniform throughout the pellet. Increasing the sintering temperature to 1075 °C results in rapid enhancement in the size of certain large grains at the expense of smaller grains and these smaller grains are interlocked between the bigger grains. It has a duplex microstructure consisting of a few very large grains in excess of 40–50 μm in size; isolated by regions consisting of fine grains (3–5 μm). The EDX analyses indicate that the composition of bigger grains is nearly stoichiometric and the smaller grains are slightly rich in copper. As the sintering temperature is increased to 1100 °C, a dramatic change occurs in the microstructure (Fig. 2c) as well as in the composition on the surface of the pellet. The smaller grains, which were rich in copper appeared to have melted, while the bigger grains remained more or less stoichiometric. The composition of the grain and the grain boundary regions shown along with the micrograph of the pellet clearly indicates that the grain

**Fig. 2** Scanning electron micrographs of  $\text{CaCu}_3\text{Ti}_4\text{O}_{12}$  ceramics sintered at (a) 1050 °C/10 h (b) 1075 °C/10 h (c) 1100 °C/10 h (d) 1120 °C/10 h



boundary region is rich in copper. Hence, the microstructural features of 1100 °C/10 h sintered sample can be broadly described as the stoichiometric grains floating in a “pool” of Cu-rich phase. On further increase in sintering temperature to 1120 °C, the Cu-rich phase appears to have recrystallised into a sheet-type morphology wherein the sheets are stacked around the grain (Fig. 2d), which is shown in the Inset of Fig. 2d. As there was a sudden change in the morphology of the pellet sintered at 1100 °C, the second set of pellets were sintered at 1100 °C for different durations to study its influence on microstructural features.

The SEM pictures of the CCTO pellets sintered at 1100 °C for increasing durations from 2.5 to 20 h are shown in Fig. 3a–e. The microstructural features of the pellet sintered at 1100 °C/2.5 h (Fig. 3a) is more or less similar to that of the pellet sintered at 1050 °C/10 h (Fig. 2a). As sintering duration is increased to 5 h, the

microstructure that is evolved (Fig. 3b) nearly resembles to that of the pellet sintered at 1075 °C/10 h (Fig. 2b). Sintering the pellet for 7.5 h and above drastically changes the microstructure, with Cu-rich phase segregating at the grain boundary. The pellets sintered for 15 and 20 h have a narrow grain size distribution with an average size of around 50 μm (Fig. 3d, e). It is intriguing to note that a closer examination of 20 h sintered CCTO ceramic reveals a fascinating microstructure in which each grain is surrounded by exfoliated sheets of Cu-rich phase (Inset of Fig. 3e). The results of elemental mapping performed on a selected area on the surface of 1100 °C/15 h sintered sample are depicted in Fig. 4a–d, which clearly shows that the pulpy region surrounding the grains is rich in Cu and deficient in Ca and Ti. The EDX pattern obtained for the grain boundary and the grain of the same region (Fig. 5a) is shown in Fig. 5b, c. The quantitative ratios of different cations are also given in the figure, which clearly demon-

**Fig. 3** Scanning electron micrographs of  $\text{CaCu}_3\text{Ti}_4\text{O}_{12}$  ceramics sintered at (a) 1100 °C/2.5 h (b) 1100 °C/5 h (c) 1100 °C/7.5 h (d) 1100 °C/15 h (e) 1100 °C/20 h

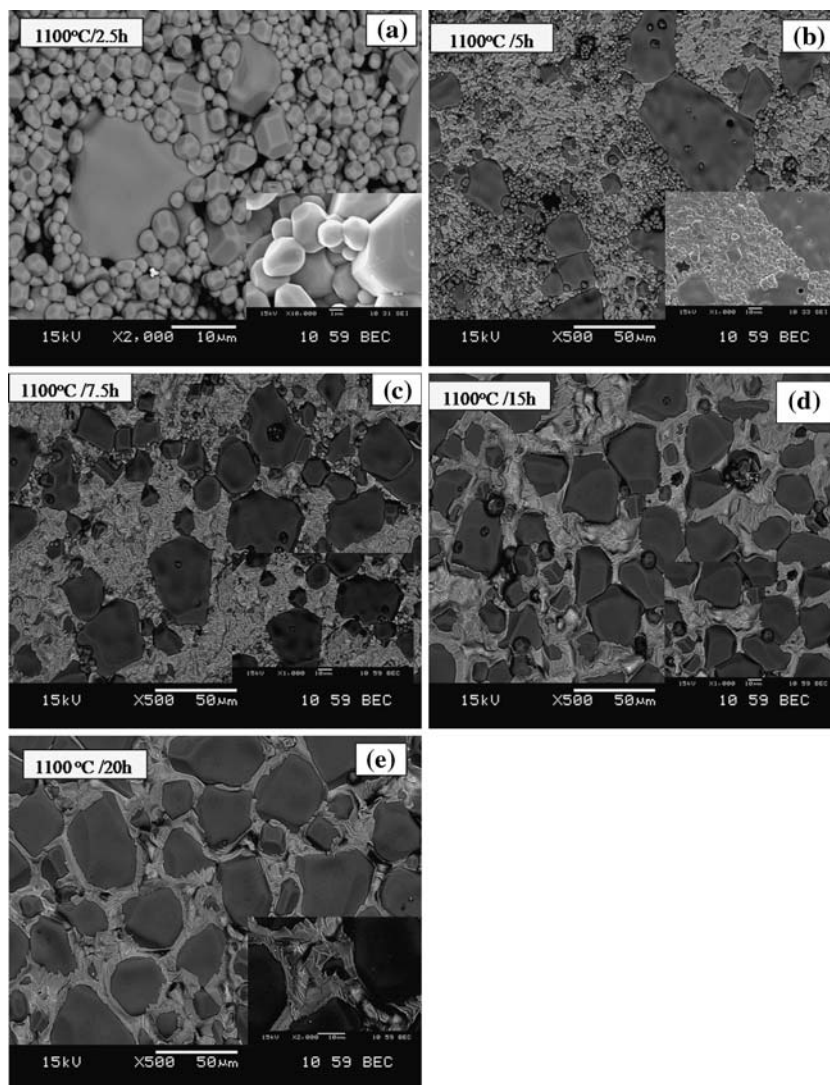
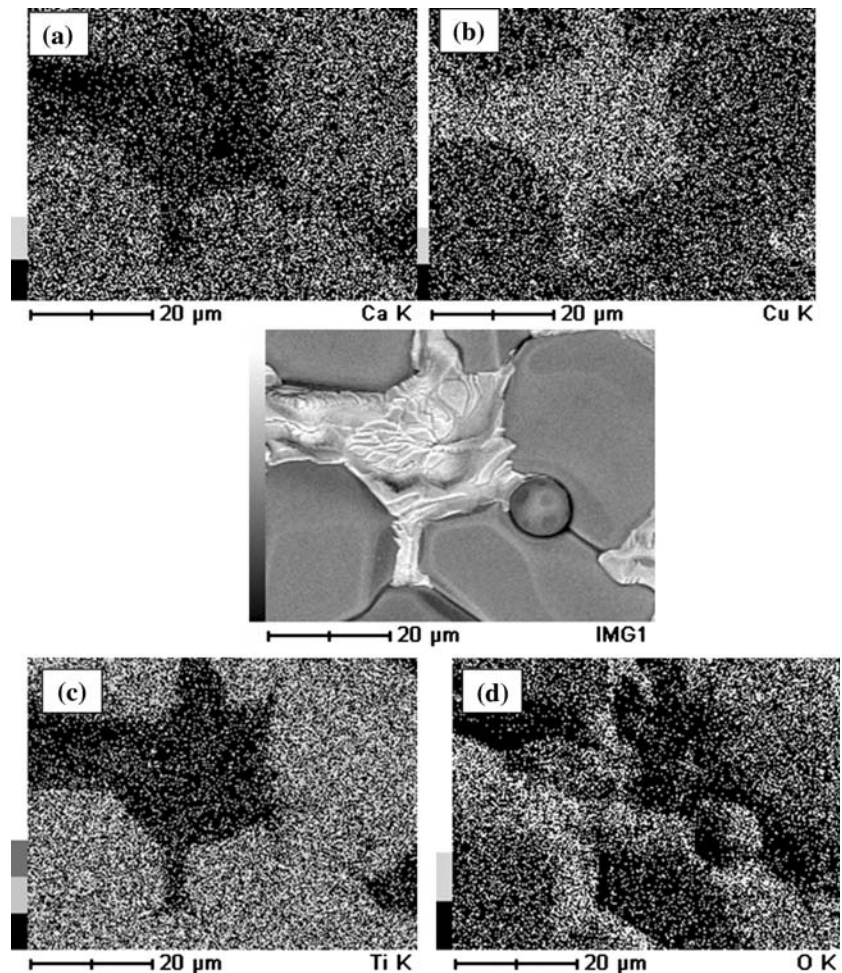


**Fig. 4** Surface distribution of different elements in the selected area of the  $\text{CaCu}_3\text{Ti}_4\text{O}_{12}$  pellet sintered at  $1100\text{ }^\circ\text{C}/15\text{ h}$  (a) Ca (b) Cu (c) Ti (d) O (Oxygen)



strate that the grain boundary region is rich in Copper, while the grain region is nearly stoichiometric.

To visualize whether the phenomenon of Cu-rich phase segregation at the grain boundary is restricted only to the surface of the sintered pellet, the microstructural analysis, EDX and the elemental analyses were performed on the fractured surface of the sintered pellet as well by probing the composition of the sample from one surface to the other through the core of the sample. The SEM micrographs of the fractured surfaces of pellets sintered at  $1075\text{ }^\circ\text{C}/10\text{ h}$  and  $1100\text{ }^\circ\text{C}/10\text{ h}$  are shown in Fig. 6a, b along with their magnified pictures of the regions corresponding to the sample surface on the fractured surface of the sample (Inset of the Fig. 6a, b). Similar to the surface morphology (Fig. 2b), fractured surface of the pellet sintered at  $1075\text{ }^\circ\text{C}/10\text{ h}$  (Fig. 6a) exhibit a duplex microstructure consisting of both fine and coarse grains. Also, as in the sample surface (Fig. 2b), the segregation of the Cu-rich phase is not observed even in the interior (Fig. 6a). In contrast, the micrograph of the fractured surfaces of the pellets sintered at  $1100\text{ }^\circ\text{C}/10\text{ h}$  (Fig. 6b) exhibits a reasonably uniform microstructure. However, unlike its

surface, the segregation of Cu-rich phase is not observed in the interior of the sample (Fig. 6b). Elemental analysis performed on a selected area of the fractured surface of the  $1100\text{ }^\circ\text{C}/10\text{ h}$  sample clearly demonstrates that the surface is rich in Cu and deficient in Ca and Ti (Fig. 7a–d).

Typical complex impedance plots ( $Z^*$  plots) at  $187\text{ }^\circ\text{C}$  for the CCTO ceramics sintered at  $1050$ ,  $1075$  and  $1120\text{ }^\circ\text{C}$  for  $10\text{ h}$  are shown in Fig. 8. The  $Z^*$  plots for the pellets sintered at  $1050$  and  $1075\text{ }^\circ\text{C}$  consist of a large semicircles with nonzero intercepts on  $Z'$  at high frequency end (Inset a of Fig. 8). These responses are in accordance with the reported  $Z^*$  plots for CCTO and could be analyzed using a simplified equivalent circuit consisting of two parallel RC elements [10, 11]. The high frequency intercept on the  $Z'$  axis corresponds to the grain resistance, whereas the diameter of the low frequency semicircle corresponds to the grain boundary resistance at  $187\text{ }^\circ\text{C}$  [10]. However, for the pellets sintered at  $1100\text{ }^\circ\text{C}$  and above for  $10\text{ h}$ , the  $Z^*$  plot exhibits two overlapping semicircles (Inset b of Fig. 8) with a nonzero intercept at the high frequency end. The  $Z^*$  plots at  $187\text{ }^\circ\text{C}$  for the pellets sintered at  $1100\text{ }^\circ\text{C}$  for different durations are shown in Fig. 9a–d. Similar to that of

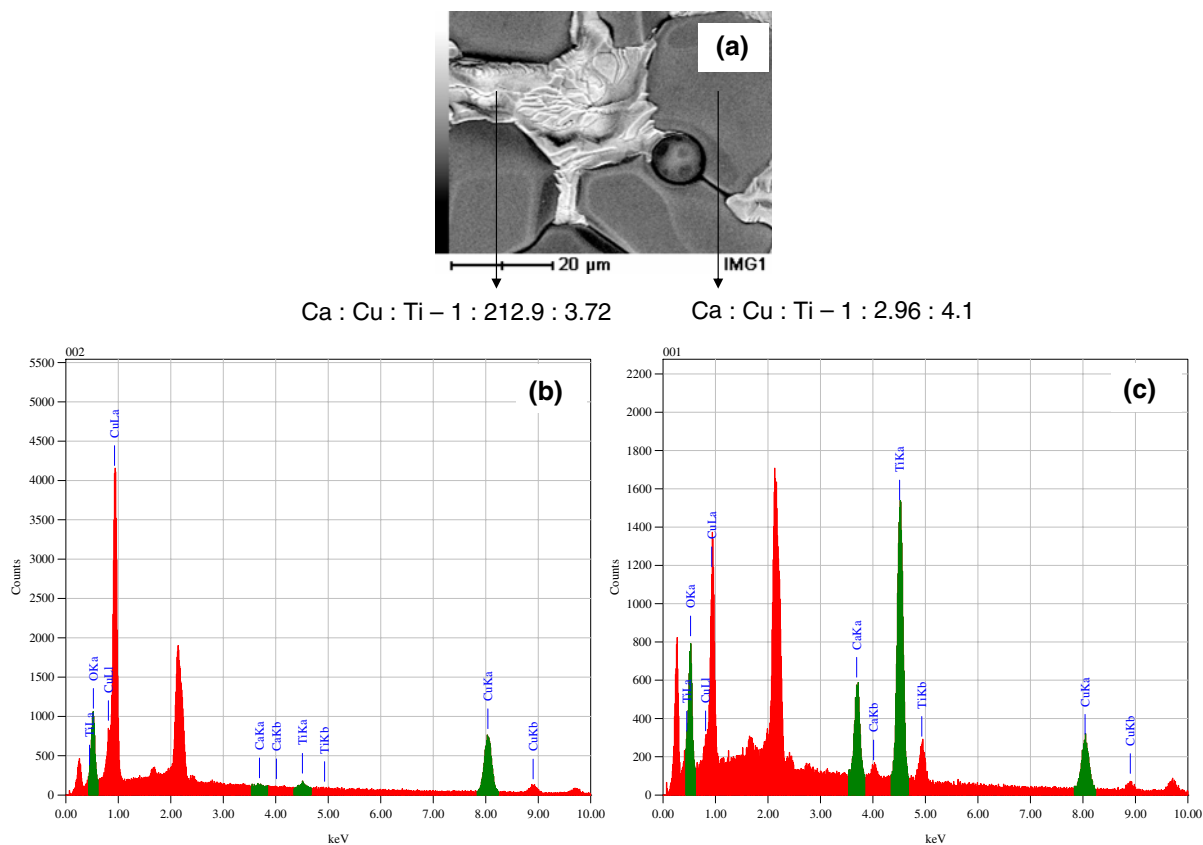
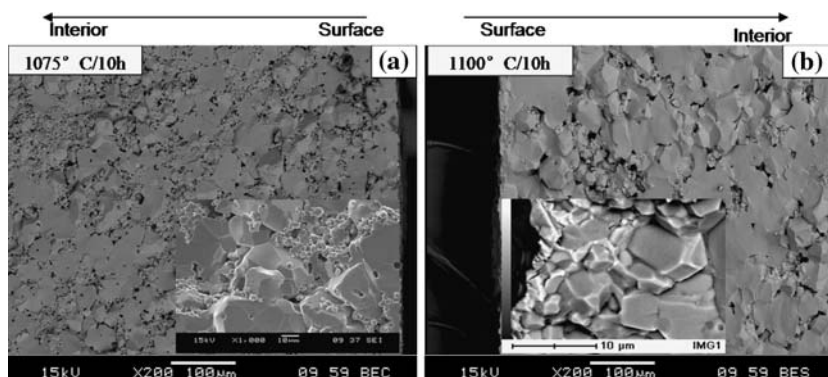


**Fig. 5** (a) SEM image of the region chosen for EDX analysis on the surface of the 1100 °C/15 h sintered sample. EDX spectrum of (b) the grain and (c) the grain boundary region on the surface of the sample

**Fig. 6** Scanning electron micrographs of the fractured surfaces of the  $\text{CaCu}_3\text{Ti}_4\text{O}_{12}$  specimens sintered at (a) 1075 °C/10 h (b) 1100 °C/10 h. Figures in the inset are the magnified pictures of the regions corresponding to the sample surface on the fractured surface of the sample



the pellet sintered at 1050 °C and below, the  $Z^*$  plots for the pellets sintered at 1100 °C for 2.5 h (Fig. 9a) and below consists of only one semicircle with a nonzero intercept on the  $Z'$ -axis at high frequency. The single semicircle in the  $Z^*$  plot is better described by the Cole-Cole equation [21].

$$Z^* = \frac{R}{1 + (i\omega\tau)^\alpha} \quad (1)$$

where  $\tau = RC$  and the parameter  $\alpha$ ,  $0 < \alpha \leq 1$ , is used to measure the departure from ideal Debye response [21].  $R$  and  $C$  are the resistance and the capacitance associated with each semicircle. For the sample sintered at 1100 °C/2.5 h, the fitted values of  $R$ ,  $C$  and  $\alpha$  for the semicircle are 3011 Ohm m,  $8.65 \times 10^{-8}$  F/m and 0.965, respectively. The value of  $\alpha$  which is close to unity suggests that the grain boundary response is grossly Debye-type in nature [21].

**Fig. 7** Distribution of various elements in the selected area of the fractured surface corresponding to the top surface of the  $\text{CaCu}_3\text{Ti}_4\text{O}_{12}$  pellets sintered at  $1100\text{ }^\circ\text{C}/10\text{ h}$  (a) Ca (b) Cu (c) Ti (d) O (Oxygen)

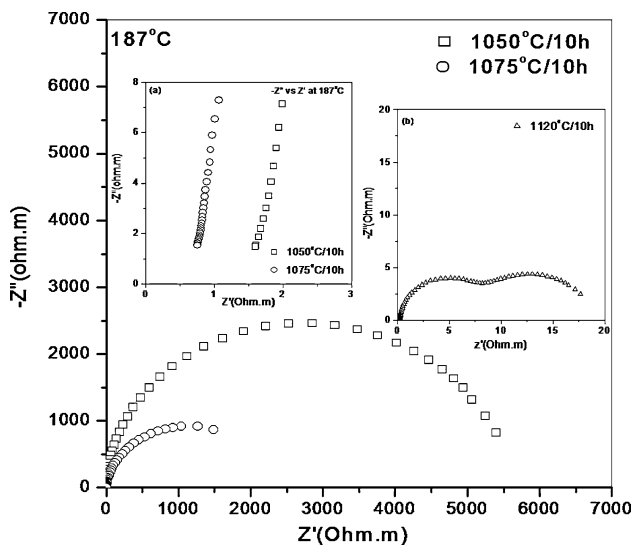
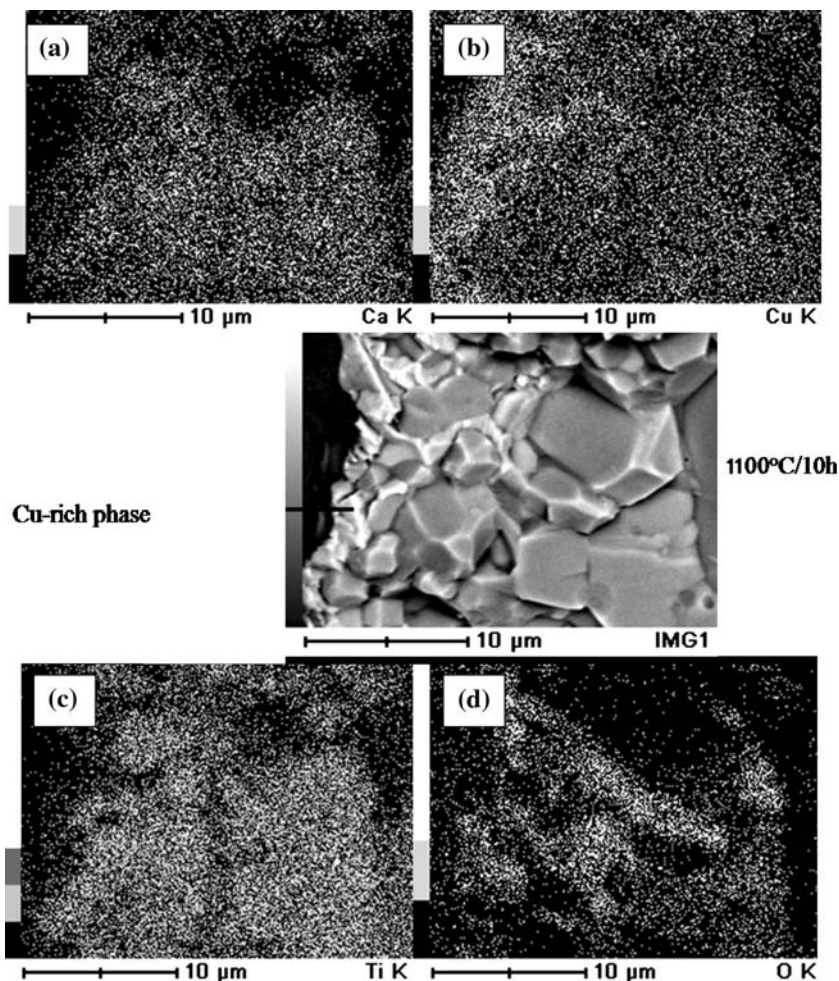
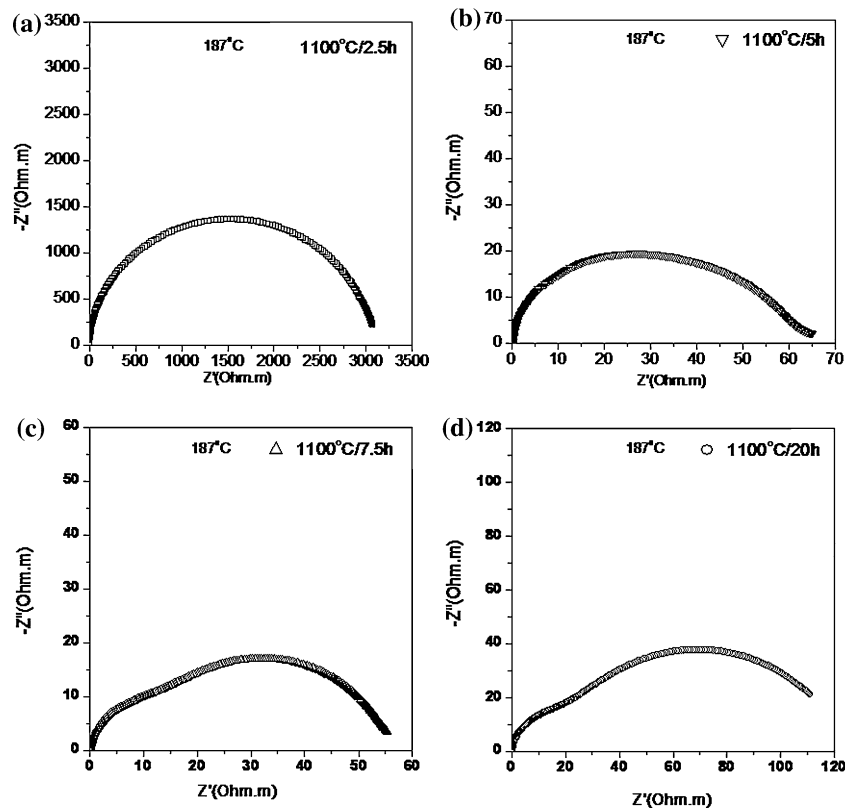


**Fig. 8** Complex impedance plot at  $187\text{ }^\circ\text{C}$  for the  $\text{CaCu}_3\text{Ti}_4\text{O}_{12}$  specimens sintered at  $1050\text{ }^\circ\text{C}/10\text{ h}$  and  $1075\text{ }^\circ\text{C}/10\text{ h}$ . The inset (a) shows the expanded view of the high frequency impedance data close to the origin for the specimens sintered at  $1050\text{ }^\circ\text{C}/10\text{ h}$  and  $1075\text{ }^\circ\text{C}/10\text{ h}$ . The inset (b) is the complex impedance plot at  $187\text{ }^\circ\text{C}$  for the specimens sintered at  $1120\text{ }^\circ\text{C}/10\text{ h}$

As the sintering duration is increased to 5 h, the  $Z^*$  response shows a depressed semicircle (Fig. 9b) which had to be fitted using an equivalent circuit consisting of three parallel RC elements connected in series as shown in Fig. 10. On further increase in the sintering duration to 7.5 h and above (Fig. 9c, d), the  $Z^*$  response clearly deconvolutes into two overlapping semicircles. For the sample sintered at  $1100\text{ }^\circ\text{C}/7.5\text{ h}$ , the fitted values of R, C and  $\alpha$  at  $187\text{ }^\circ\text{C}$  for high and low frequency semicircles are  $6.45\text{ Ohm m}$ ,  $1.59 \times 10^{-7}\text{ F/m}$ , 1 and  $50.88\text{ Ohm m}$ ,  $1.57 \times 10^{-5}\text{ F/m}$  and 0.73, respectively. Hence, the resistance and the capacitance of the circuit elements associated with the semicircle at the low frequency end are much higher than that of the values associated with the semicircle at the high frequency end. Moreover, the value of  $\alpha$  for the two regions suggests that the high frequency semicircle is more of Debye-type than the semicircle at the low frequency end.

A closer observation of SEM micrographs of the pellets with different sintering conditions and their corresponding  $Z^*$  response reveals the existence of a close relation

**Fig. 9** Complex impedance plot at 187 °C for the  $\text{CaCu}_3\text{Ti}_4\text{O}_{12}$  specimens sintered at (a) 1100 °C/2.5 h (b) 1100 °C/5 h (c) 1100 °C/7.5 h (d) 1100 °C/20 h



between them. It is intriguing to note that the additional semicircle at the low frequency end appears only for those samples which have the segregation of the Cu-rich phase on the surface of the sample, such as the pellet sintered at 1100 °C/15 h. Hence, the appearance of the additional semicircle is tentatively ascribed to the presence of Cu-rich phase on the surface, as its electrical response might be different from that of the rest of the sample. To examine the influence of the electrode/Sample contact effect on the additional semicircle,  $Z^*$  measurements were carried out on the pellets sintered at 1100 °C/15 h with different electrode materials such as sputtered Au, Ag and Al. No difference in impedance response was observed on using different electrode materials and hence ruled out the possibility of electrode depletion effects.

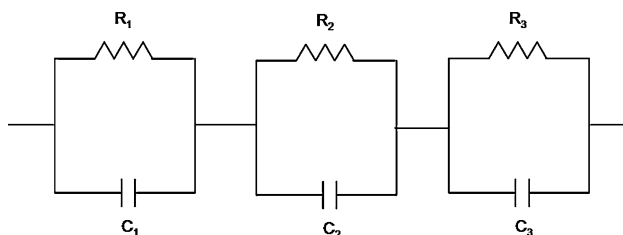


**Fig. 10** Modified equivalent circuit model to describe the electrical properties of  $\text{CaCu}_3\text{Ti}_4\text{O}_{12}$  ceramics

To corroborate the above observations, a pellet was sintered at 1100 °C/40 h to ensure the presence of Cu-rich phase segregation on the surface of the sample. The  $Z^*$  plot at 187 °C for the as-sintered sample (1100 °C/40 h) clearly reveals the existence of two semicircles, with the resistance and the capacitance associated with the low frequency semicircle being much higher than those of the high frequency semicircle (Fig. 11). Since the segregation of Cu-rich phase was observed only on the surfaces, the sample was evenly polished on either side, which interestingly led to the complete disappearance of the additional semicircle in  $Z^*$  plots (thickness reduced from 1.85 to 1.5 mm). On further reducing the thickness evenly on either side by another 0.5 mm, the diameter of the semicircle at the high frequency end decreases.

The above-mentioned samples were also analyzed using the combined spectroscopic plots of the imaginary components of the impedance,  $Z''$ , and electric modulus,  $M''$ , due to its ability to effectively separate out the electroactive regions as shown in Fig. 12a, b and 13a, b. The most resistive element dominates the  $Z''$  plot, while the element with low capacitance dominates the  $M''$  plot. The combined  $-Z''$ ,  $M''$  spectroscopic plots for the pellets sintered at 1100 °C/2.5 h (Fig. 12a) shows the presence of only one Debye-like peak in each spectrum and the high frequency incline in the  $M''$  spectrum. This suggests the presence of only two electroactive regions in the sample, i.e., one with

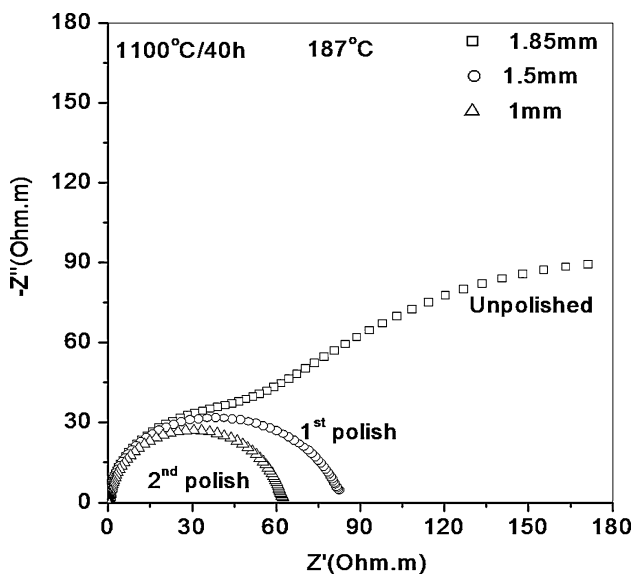


**Fig. 11** Complex impedance plot at 187 °C for the as-sintered  $\text{CaCu}_3\text{Ti}_4\text{O}_{12}$  specimen at 1100 °C/40 h and for the polished samples

low resistance and low capacitance (Grain) and the other with high resistance and high capacitance (Grain boundary). On the other hand, the combined  $-Z''$ ,  $M''$  plots for the pellet sintered at 1100 °C/15 h (Fig. 12b) shows the presence of two Debye-like peaks in  $-Z''$ -plot and  $M''$  spectrum consist of single Debye-like peak with a high frequency incline. The  $Z''$  plot is dominated by the most resistive element, i.e., response due to the surface segregation,  $R_{\text{Su}}$  (Indicated by \*), whereas the  $M''$  plot is dominated by the element with relatively smaller capacitance ( $C_{\text{gb}}$ ), i.e., the grain boundary (Indicated by #). In the  $Z''$  plot, the peak corresponding to the grain boundary appears only as a shoulder (Indicated by \*) due to its relatively low resistance, as compared to that of the surface layer resistance ( $R_{\text{Su}}$ ). In the  $M''$  plot, the response from the surface layer is completely masked by the response from the grain boundary layer due to the high capacitance associated with the surface layer ( $C_{\text{Su}}$ ). The downward arrow mark in Fig. 12b is to indicate that the strong peak in  $M''$  plot due to grain boundary response appears only as a shoulder in  $Z''$  plots. Figure 13a, b shows the combined ( $-Z''$ ,  $M''$ ) spectroscopic plots for the unpolished and polished samples. The response from the unpolished sample consists of two Debye-like peaks in  $Z''$  spectrum (One due to surface layer and other due to grain boundary), whereas the polished sample consists of only one Debye-like peak (Only due to grain boundary) similar to the pellet sintered at 1100 °C/2.5 h. The downward arrow mark in Fig. 13a is to indicate that the strong peak in  $M''$  plot due to grain boundary response appears only as a shoulder in  $Z''$  plot. These observations clearly suggest that the low frequency semicircle is due to the segregation of the Cu-rich phase on the

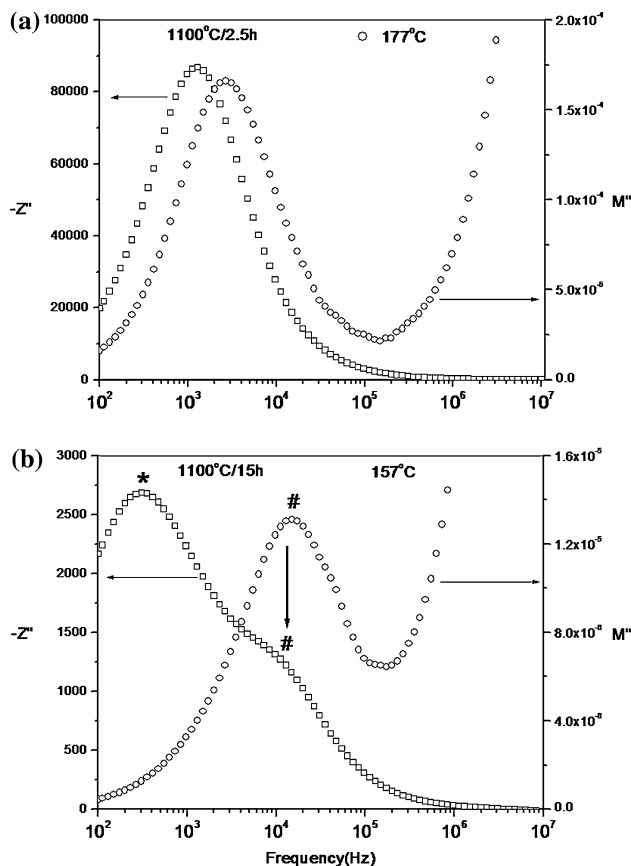


**Fig. 12** Combined ( $Z''$ ,  $M''$ ) spectroscopic plot for the  $\text{CaCu}_3\text{Ti}_4\text{O}_{12}$  ceramics sintered at (a) 1100 °C/2.5 h at 177 °C (b) 1100 °C/15 h at 157 °C

surface and the semicircle at high frequency end arises from the grain boundary region.

To further substantiate these results, both Cu-rich ( $\text{CaCu}_{3.2}\text{Ti}_4\text{O}_{12}$ ) and Cu-deficient ( $\text{CaCu}_{2.8}\text{Ti}_4\text{O}_{12}$ ) samples were prepared and sintered at 1100 °C/10 h. Microstructure and impedance responses of these samples are shown in Fig. 14a–d. As expected, the grain boundary regions at the surface of the Cu-rich samples are copious in copper content and its  $Z^*$  response consists of two semicircles. On the other hand, the Cu-deficient sample consists of very small grains (3–5  $\mu\text{m}$ ) without the segregation of Cu-rich phase on the surface. This sample shows only one semicircle corresponding to the grain boundary region, thus confirming that the Cu-rich phase at the surface is responsible for the observation of low frequency semicircle.

To investigate further, whether the copper segregation at the surface and the appearance of concurrent semicircle at the low frequency end is limited only to CCTO in the  $\text{ACu}_3\text{M}_4\text{O}_{12}$  (A = alkali, alkaline-earth metal, rare-earth metal or vacancy, M = transition metal) family of oxides,

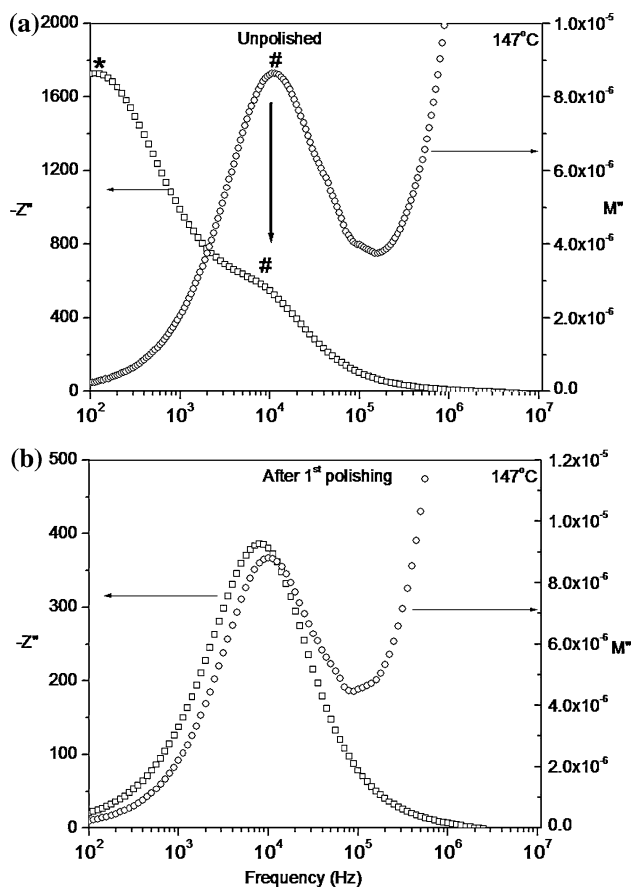
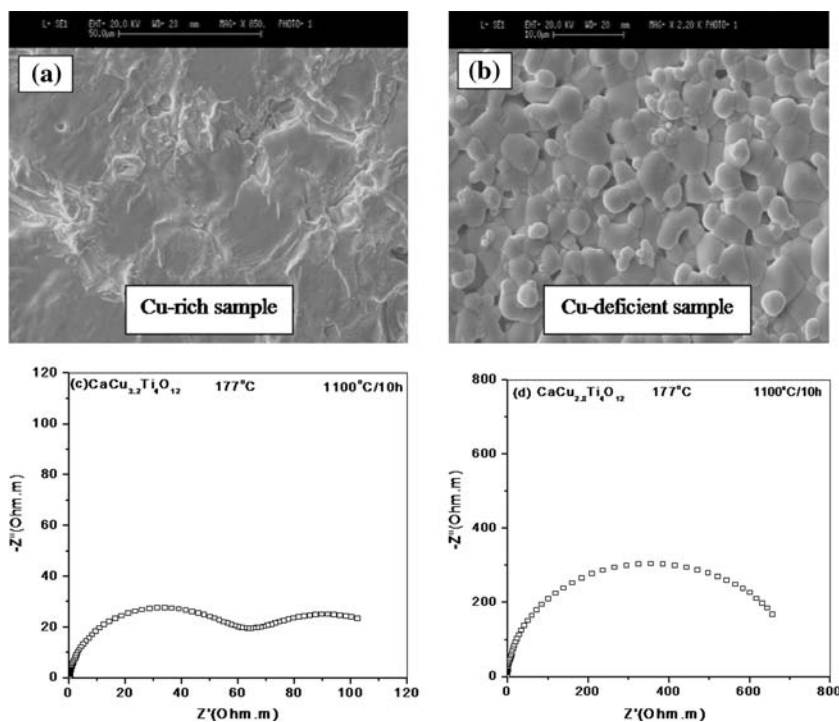


**Fig. 13** Combined ( $Z''$ ,  $M''$ ) spectroscopic plot at 147 °C for the  $\text{CaCu}_3\text{Ti}_4\text{O}_{12}$  sample sintered at 1100 °C/40 h for (a) Unpolished and (b) the polished sample

**Fig. 14** (a & b) Scanning electron micrographs of the Cu-rich and Cu-deficient  $\text{CaCu}_3\text{Ti}_4\text{O}_{12}$  samples. c&d are the Complex impedance plots at 177 °C for the Cu-rich and Cu-deficient samples



low dielectric constant member of the family,  $\text{La}_{2/3}\text{Cu}_3\text{Ti}_4\text{O}_{12}$  (LCTO), was chosen for further investigations. The SEM micrograph and  $Z^*$  plots of LCTO ceramics sintered at 1100 °C/40 h are shown in Fig. 15a, b. The microstructure of LCTO is distinctly different from that of CCTO as its grains have smooth faces associated with cubic appearance without the segregation of Cu-rich phase at the grain boundaries. As anticipated,  $Z^*$  plots of LCTO show only one semicircle corresponding to the grain boundary with a nonzero intercept on the  $Z'$ -axis at the high frequency end. All these experiments clearly confirm that the semicircle at the low frequency end in the  $Z^*$  plots of CCTO originate from the segregation of Copper particularly on the surface.

## Conclusions

Polycrystalline CCTO ceramics were prepared by conventional solid-state reaction route and were sintered at different temperatures and durations. Microstructure and impedance analyses were performed on all the samples. The microstructure of the sintered ceramic was strongly dependent on sintering temperature and its duration. The samples that were sintered at lower temperature and for shorter durations consisted of small grains, while samples that were sintered at higher temperatures and longer durations consisted of larger grains (50–60  $\mu\text{m}$ ) associated with the segregation of Cu-rich phase at the grain boundary

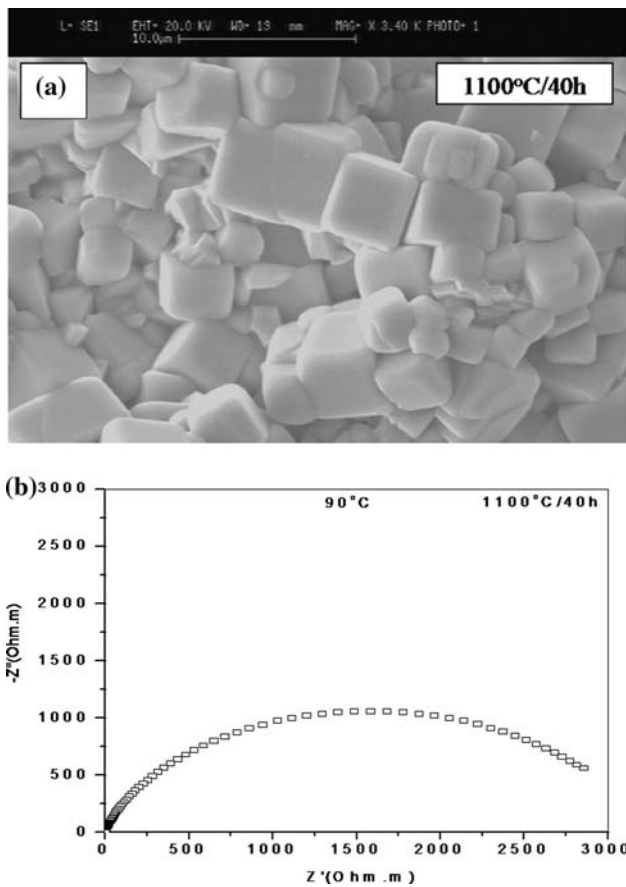


**Fig. 15** (a) Scanning electron micrographs of  $\text{La}_{2/3}\text{Cu}_3\text{Ti}_4\text{O}_{12}$  ceramics sintered at  $1100\text{ }^\circ\text{C}/40\text{ h}$  (b) Complex impedance plot at  $90\text{ }^\circ\text{C}$  for  $\text{La}_{2/3}\text{Cu}_3\text{Ti}_4\text{O}_{12}$  ceramics sintered at  $1100\text{ }^\circ\text{C}/40\text{ h}$

particularly on the surface. The impedance plots of the sample that were sintered at lower temperatures exhibited only one semicircle, corresponding to the grain boundary, with the nonzero intercept at the high frequency end corresponding to the grain. The samples that were sintered at higher temperatures and for longer durations exhibited an additional semicircle, which was attributed to the Cu-rich phase segregating at the surface of the sample. The complete vanishing of the additional semicircle for the evenly polished sample endorsed that the Cu-rich phase is

responsible for the occurrence of the additional semicircle. These observations were further verified and confirmed by preparing Cu-deficient and Cu-rich CCTO ceramics. The Cu-deficient sample exhibited only one semicircle, while the Cu-rich samples exhibited two semicircles confirming the role of Cu-rich phase on the appearance of additional semicircle and on the overall electrical behavior of CCTO ceramics.

## References

1. Biskup N, De Andres A, Martinez JL, Perca C (2005) *Phys Rev B* 72:24115
2. Kim B-G, Cho SM, Kim T-Y, Jang HM (2001) *Phys Rev Lett* 86:3404
3. Raevski IP, Prosandeev SA, Bogatin AS, Malitskaya MA, Jastrabik L (2003) *J Appl Phys* 93:4130
4. Wang J, Tang XG, Chan HLW, Choy CL, Luo H (2005) *Appl Phys Lett* 86:152907
5. Wu J, Nan C-W, Lin Y, Deng Y (2002) *Phys Rev Lett* 89:217601
6. Cohen RE (1992) *Nature* 358:136
7. Subramanian MA, Li D, Duan N, Reisner BA, Sleight AW (2000) *J Solid State Chem* 151:323
8. Ramirez AP, Subramanian MA, Gardel M, Blumberg G, Li D, Vogt T, Shapiro SM (2000) *Solid State Commun* 115:217
9. Homes CC, Vogt T, Shapiro SM, Wakimoto S, Ramirez AP (2001) *Science* 293:673
10. Sinclair DC, Adams TB, Morrison FD, West AR (2002) *Appl Phys Lett* 80:2153
11. Adams TB, Sinclair DC, West AR (2002) *Adv Mater* 14:1321
12. Zang G, Zhang J, Zheng P, Wang J, Wang C (2005) *J Phys D* 38:1824
13. Bender BA, Pan M-J (2005) *Mater Sci Eng B* 117:339
14. Cohen MH, Neaton JB, He L, Vanderbilt D (2003) *J Appl Phys* 94:3299
15. Lunkenheimer P, Fichtl R, Ebbinghaus SG, Loidl A (2004) *Phys Rev B* 70:172102
16. Lei Zhang Z-JT (2004) *Phys Rev B* 70:174306
17. West AR, Adams TB, Morrison FD, Sinclair DC (2004) *J Eur Ceram Soc* 24:1439
18. Chiodelli G, Massarotti V, Capsoni D, Bini M, Azzoni CB, Mozzati MC, Lupotto P (2004) *Solid State Commun* 132:241
19. Zhang L (2005) *Appl Phys Lett* 87:022907
20. Zhang JL, Zheng P, Wang CL, Zhao ML, Li JC, Wang JF (2005) *Appl Phys Lett* 87:142901
21. Macdonald JR (1987) *Impedance spectroscopy*. Wiley, New York